Electronic Supplementary Material (ESI) for Journal of Materials Chemistry A.


# Supporting Information

## In situ structural evolution of a nickel boride catalyst: synergistic geometric and electronic optimization for the oxygen evolution reaction

Jihong Li, Hui Chen, Yipu Liu, Ruiqin Gao and Xiaoxin Zou*

State Key Laboratory of Inorganic Synthesis and Preparative Chemistry, College of Chemistry, Jilin University, Changchun 130012, P. R. China

*Corresponding author. E-mail: xxzou@jlu.edu.cn

## Experimental section

**Chemicals and Reagents.** Ni plate (thickness: 0.3 mm) was purchased from Northeast Special Steel Refco Group Ltd. Prior to the use, Ni plate was cleaned sequentially with acetone, and deionized water several times. Ethyl alcohol and Potassium hydroxide (KOH) were purchased from Beijing Chemical Factory. Nafion® perfluorinated resin solution was purchased from Sigma-Aldrich. Amorphous boron powder was purchased from Shanghai Macklin Biochemical Co., Ltd. Sodium hydroxide (NaOH) and Nickel nitrate hexahydrate ($Ni(NO_3)_2 \cdot 6H_2O$) were purchased from Sinopharm Chemical Reagent Co., Ltd. Highly purified water (> 18 MΩ cm resistivity) was provided by a PALL PURELAB Plus system.

**Sample Preparation.** Boronized Ni in-situ grown on Ni plate was synthesized via a facile reaction between Ni plate and boron powder. Typically, a piece of nickel plate (5cm×0.8cm×0.3mm) was embedded in boron powder (4.0 g), which was placed in a quartz tube and then annealed at 800 °C for 40 min under $N_2$ atmosphere at a heating rate of 3 °C $min^{-1}$. In this process, the nickel plate acts as Ni source as well as scaffold. What's more, almost no boron powder was oxidized under nitrogen atmosphere hence boron powder can be reused many times without impact on the final products.

**Characterization.** The powder X-ray diffraction (XRD) patterns were recorded on a Rigaku D/Max 2550 X-ray diffractometer with Cu K$\alpha$ radiation ($\lambda$ = 1.5418 Å). The scanning electron microscope (SEM) images were performed on a JEOL JSM 6700F electron microscope at an accelerating voltage of 5 kV. The Energy dispersive

X-ray (EDX) analysis was carried out using an EDX system attached to JEOL JSM-7800F scanning electron microscopy. The X-ray photoelectron spectroscopy (XPS) was collected on an ESCALAB 250 X-ray photoelectron spectrometer with a monochromatic X-ray source (Al K$\alpha$ $h\upsilon$ = 1486.6 eV). Inductively coupled plasma atomic emission spectroscopy (ICP-OES) was performed on a Perkin-Elmer Optima 3300DV ICP spectrometer. The transmission electron microscope (TEM) images were taken on a Philips FEI Tecnai G2S-Twin microscope equipped with a field emission gun operating at 200 kV. The Raman spectra of the materials were obtained with a Renishaw Raman system model 1000 spectrometer operating with a 20 mW air-cooled argon ion laser (532 nm) as the excitation light source. Electrical resistivity was measured used the Van Der Pauw method with four probes

**Electrochemical measurements.** All electrochemical measurements were performed in a standard three-electrode configuration with a CH Instrument (Model 650E). The electrochemical cell was a plastic cell with a diameter of 4 cm and a height of 8 cm. The as prepared $Ni_3B$ catalyst with a working surface area of 0.2 $cm^2$ was directly used as a working electrode and Ni plate is coated with hot melt adhesive except for the working area to ensure the accuracy of the working area. A Hg/HgO electrode and a Pt wire electrode were employed as reference and counter electrodes, respectively. Before testing, the Hg/HgO reference electrode was calibrated according to our previously reported publication.[1] To avoid the influence of trace Fe on the activity of $Ni_3B$, the electrolyte was purified to remove the iron impurity according the report published by Boettcher.[2] For linear sweep voltammetry (LSV) measurements, the scan

rate was set to 1 mV $s^{-1}$. During the test, the corresponding single-point impedance was used to estimate the resistances of the test system along with bubbling $N_2$ and compensated by 85% *iR*-compensations. In order to determine the stability of the catalyst, chronopotentiometric measurements were performed at a current density of 10 mA $cm^{-2}$ without *iR*-compensations. The conversion between the Hg/HgO reference and RHE in 1M KOH solution was established using equation (1):

$$E_{RHE} = E_{Hg/HgO} + 0.924\ V \qquad (1)$$

In order to determine whether boron ions were leached out when testing, we used ICP-OES to detect the boron ions in 1M KOH solution during the long-time electrolysis process at 10mA $cm^{-2}$ at the presence of boronized Ni. The electrolyte was collected after 15, and 350 h during operation, and the results shown in Table S1 reveal that no recognizable boron species are present in the electrolyte.

Estimation of effective electrode surface area. To estimate the corresponding effective electrode surface areas, cyclic voltammetry (CV) measurements were recorded to analyze the electrochemical double layer capacitance of various samples at non-faradaic overpotentials. In details，a series of CV measurement were performed at various scan rates (10, 20, 30, 40 mV $s^{-1}$ and etc.) from 1.024 to 1.124 V *vs* RHE. The sweep segments were set to 10. A linear trend can be observed by plotting the difference in current density (*j*) between the anodic and cathodic ($\Delta j$) against the scan rate. The geometric double layer capacitance ($C_{dl}$), a value coinciding with the effective electrode surface area (ECSA) of the material, was equal to half of the slope of the fitted line. Based on this $C_{dl}$ values, we can calculate the ECSA of different materials by equation (2):

$$\mathrm{EASA} = \frac{C_{dl}}{C_S} \times \mathrm{ASA} \qquad (2)$$

where $C_s$ is the specific capacitance and ASA is the actual surface area of the electrode. The value of $C_s$ is 0.04 mF $cm^{-2}$ of this work.

Measurements of electrochemical impedance spectroscopy (EIS). Electrochemical impedance spectroscopy (EIS) was performed on the materials at the operating conditions for OER. The initial potential was set to 1.55 V *vs* RHE. In the test, the sinusoidal voltage of amplitude was 5 mV and the scanning frequency ranged from 10,000 to 1 Hz. The EIS of material was then fitted by a simplified Randles equivalent circuit.

Determination of Faradaic yield. The Faraday efficiency of catalyst about the OER is obtained from the ratio of the amount of oxygen evolved experimentally to the amount of oxygen produced theoretically during OER process. To calculate the Faraday efficiency, the oxygen produced by the reaction is collected by the drainage method, and then the amount of oxygen (in mol) is calculated using the ideal gas law. The corresponding theoretical amount of oxygen, which was calculated by assuming that the working electrode 100% current output during the reaction is for OER, was determined by Faraday's law.

pH Dependence Studies.The potential of steady state electrode was tested by Chronopotentiometric at a current density of 1mA $cm^{-1}$ in different concentrations KOH solutions, whose pH were 12.36, 12.93 13.29, and 13.89. The recorded potentials (*vs* Hg/HgO) were converted according to the equation (3):

$$E_{NHE} = E_{Hg/HgO} + 0.924 \qquad (3)$$

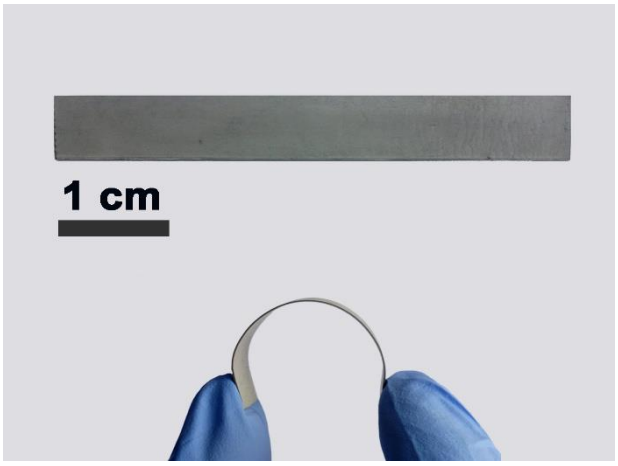


**Figure S1.** Digital images of boronized Ni.

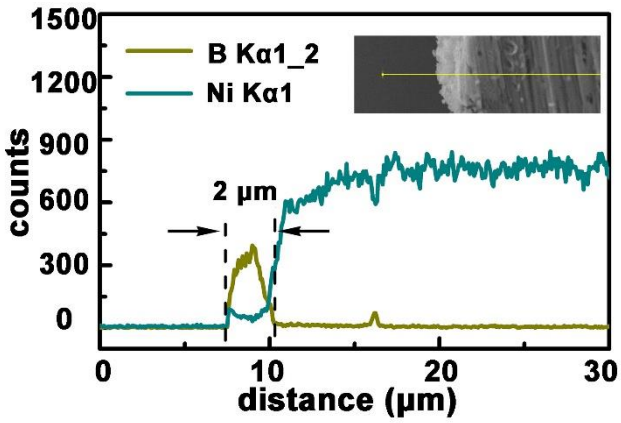


**Figure S2.** SEM-EDX line scanning profiles of Ni and B along the line drawn across the cross section (the inset) of boronized Ni， and the distance of the parallel dotted line was ~2 μm.

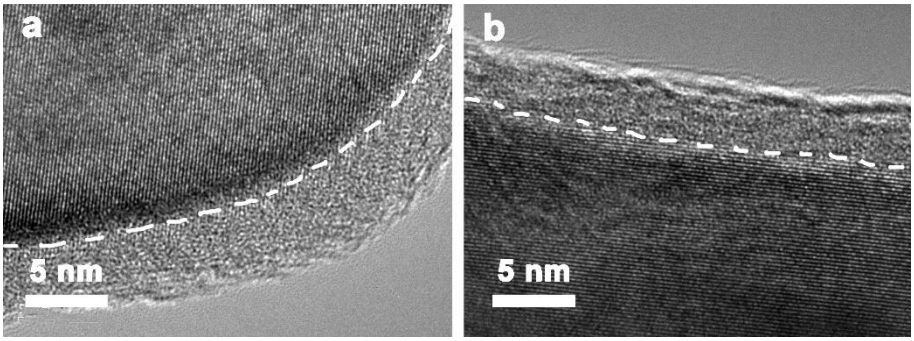


**Figure S3.** (a, b) TEM images of boronized Ni with 3-5 nm amorphous layer.

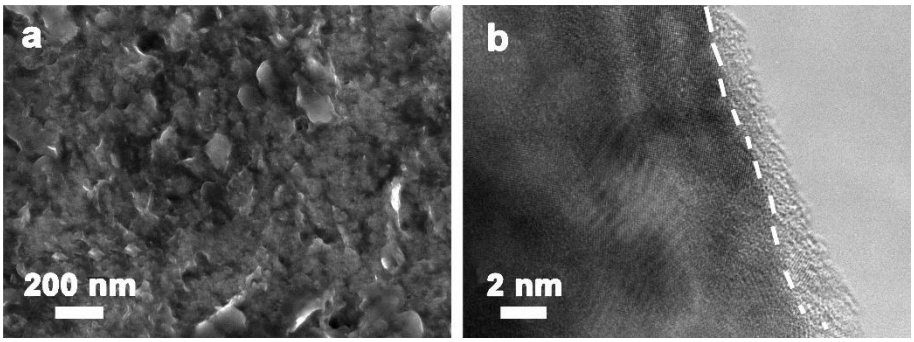


**Figure S4.** (a) SEM image, (b) HRTEM image of the pristine Ni after OER.

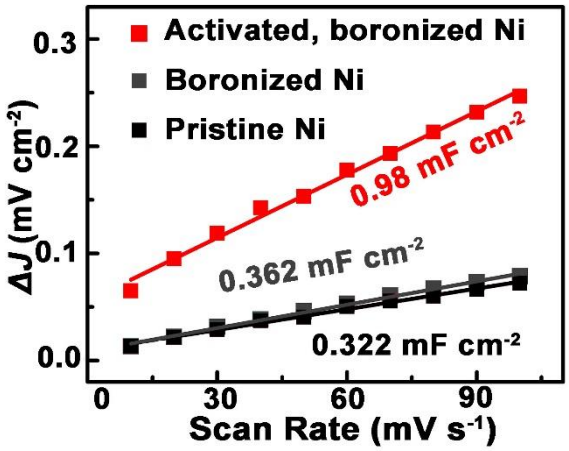


**Figure S5.** The difference of current density between the anodic and cathodic sweeps versus scan rate; the slope of the fitting line is used for determination of the double-layer capacitance ($C_{dl}$) which is used to calculate ECSA of the catalysts.

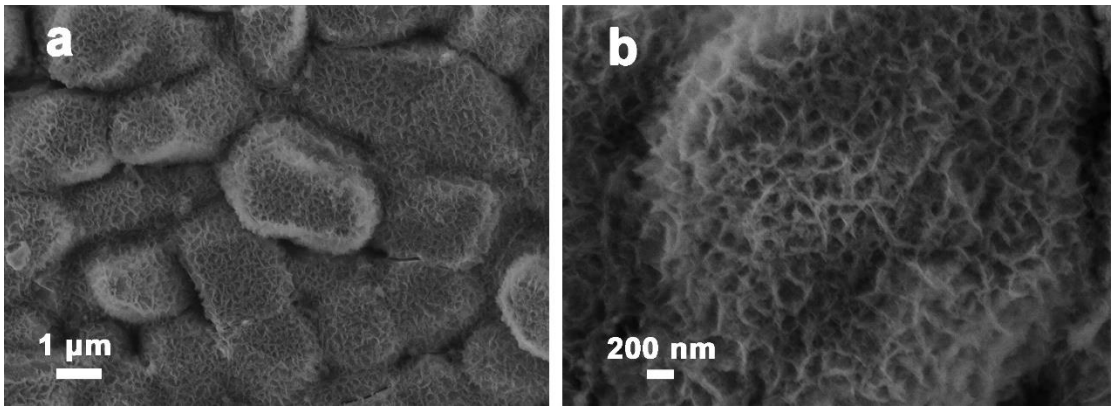


**Figure. S6.** SEM images of activated, boronized Ni after 150 h-long term stability test.

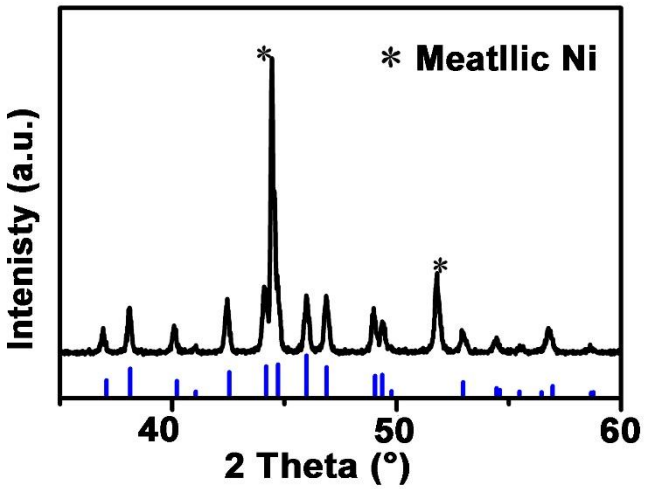


**Figure. S7.** XRD patterns of activated, boronized Ni after 150 h-long term stability test

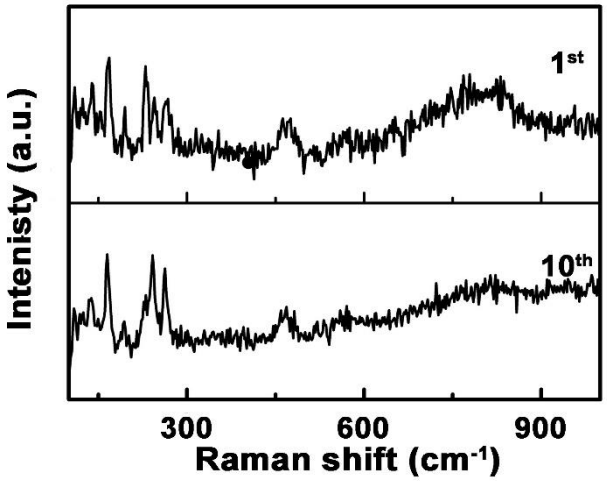


**Figure S8.** Raman spectra of the boronized Ni-1 and boronized Ni-10.

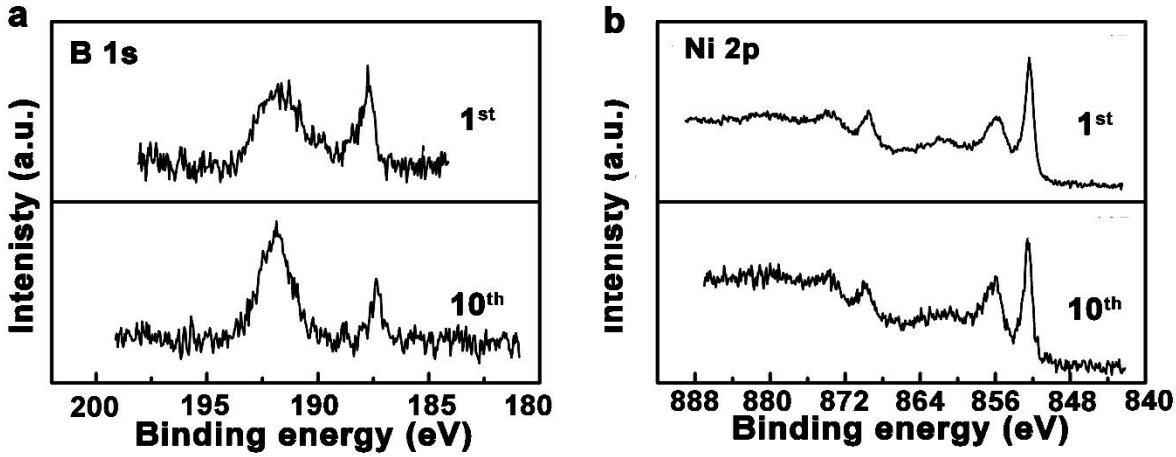


**Figure S9. (a)** B 1s XPS spectra, (b) Ni 2p XPS spectra of of the boronized Ni-1 and

boronized Ni-10.

**Table S1.** Ion concentration of boron in electrolyte during the long-time electrolysis process at 10 mA $cm^{-2}$ at the presence of boronized Ni.

| time (h) | boron ion concentration (mol $L^{-1}$) | %RSD[a] (boron) |
|---|---|---|
| 15 | $7.95\times10^{-7}$ | 16.00 |
| 350 | $4.62\times10^{-7}$ | 1.720 |

a: RSD is related to the relative standard deviation

## Reference


1 Y. Liu, X. Liang, L. Gu, Y. Zhang, G. D. Li, X. Zou, J. S. Chen, *Nat. Commun.* 2018, **9**, 2609.

2 L. Trotochaud, S. L. Young, J. K. Ranney, S. W. Boettcher, *J. Am. Chem. Soc.* 2014, **136**, 6744.